Experimental study of soft porous lubrication

Zenghao Zhu
Villanova Cellular Biomechanics and Sports Science Laboratory, Villanova, Pennsylvania 19085, USA and Department of Mechanical Engineering, Villanova University, Villanova, Pennsylvania 19085, USA

Sheldon Weinbaum
Department of Biomedical Engineering, City College of New York, New York, New York 10031, USA

Qianhong Wu*
Villanova Cellular Biomechanics and Sports Science Laboratory, Villanova, Pennsylvania 19085, USA and Department of Mechanical Engineering, Villanova University, Villanova, Pennsylvania 19085, USA

(Received 15 March 2018; revised manuscript received 10 August 2018; published 26 February 2019)

In this paper, we report an experimental study to examine the lift generation and friction reduction using soft porous media. The study is inspired by the frictionless motion of a red blood cell gliding over the highly porous endothelial glycocalyx layer that covers the inner surface of our blood vessels. The experimental setup consists of a running conveyer belt coated with a soft porous sheet and an upper fully instrumented planar board, i.e., a planing surface. Both the lubrication pressure and the sliding friction are measured. The results clearly demonstrate a huge potential for using highly compressible porous media for a new generation of soft bearings with tremendously increased pore pressure and infinite life.

DOI: 10.1103/PhysRevFluids.4.024305

I. INTRODUCTION

Friction is a major contributor to the energy loss and inefficiencies in mechanical systems. Anywhere that moving parts exist, from large-scale wind turbines to small-scale microfluidic devices, friction presents to scavenge energy [1]. Therefore, methods to reduce friction are of paramount importance to the safe, reliable, and efficient operation of mechanical systems. Through years of evolution, nature has created a model for us to follow to tremendously reduce friction. At the luminal side of the endothelial cells lies a soft, porous, hydrated endothelial glycocalyx layer (EGL) of glycoproteins and proteoglycans [2–5]. An intriguing phenomenon is that a red blood cell (RBC) can glide over the EGL almost without friction in a tightly fitting capillary. A possible mechanism behind the mystery, was proposed in Ref. [6] and Refs. [5,7,8]. In Ref. [6], a generalized lubrication theory was developed, which shows that the excess pore pressure generated by a planing surface moving on any compressible porous media scales as $\alpha^2 = h_2^2/K_{p2}$, where α is the Brinkman parameter, h_2 and K_{p2} are the thickness and the Darcy permeability of the porous layer at the leading edge, respectively. α is of order 10^2 or larger for RBCs gliding on the EGL. Thus, the lift forces can be four or more orders of magnitude greater than classical lubrication theory. The same mechanism is applied to a human skiing or snowboarding on fresh snow powder, which has an unexpected hydrodynamic similarity to the motion of a RBC. The dramatic increase in lift is due to the fact that

*qianhong.wu@villanova.edu

 ©2019 American Physical Society

the fluid is transiently trapped within the soft porous material and can't escape on the timescale of the motion. Weinbaum *et al.* [9] predicts that the elastic restoring force of the core proteins of the EGL [10] is at most 5% of the pore pressure when the RBC is moving at velocities of even a few μm/s. Thus, the frictional drag from the solid phase will be dramatically reduced since most of the load is supported, not by the fibers, but by the fluid pore pressure.

The theories in Refs. [6,9] show an exquisite design of the nature. However, they do not provide a rigorous basis for evaluating their accuracy or limitations. Despite extensive studies [11–28], the concept of soft porous lubrication has not yet been proved experimentally. One would ask: Can we create similar superlubrication conditions with tremendously reduced friction as those observed in microcirculation? The current study is aimed at answering this question.

II. EXPERIMENTAL SETUP

Figure 1(a) shows the problem schematic, where a planing surface glides over a soft porous layer at a velocity, U. The porous layer thicknesses under the trailing ($x/L = 0$) and leading ($x/L = 1$) edges are h_1 and h_2, respectively, and the undeformed porous layer thickness is h_0. Here L is the length of the planing surface. Figure 1(b) shows the detailed design of the experimental setup, where a fibrous porous layer, namely, "material P," is attached to a conveyor belt that is moved at velocity U, and a planar board is held fixed above the porous layer serving as the planing surface. Material P, made of 100% polyester with fiber diameter being around 18 μm, has an undeformed porosity, $\phi_0 = 0.994$, and permeability, $K_{p0} = 3.7 \times 10^{-8}$ m^2 [28,29].The conveyor belt is driven by two rollers connected to a DC electric motor (Inertial Motors Corp., Model D30L). Two nylon sidewalls are mounted to the frame to seal along the edge of the planing surface to eliminate pressure leakage in the lateral direction, forming a one-dimensional pressure distribution, similar to that observed in the motion of RBCs in a tightly fitting capillary.

The instrumentation is shown in Fig. 1(c). Three load cells, L_i ($i = 1, 2, 3$) (Futek. Model FBB350), were mounted at three different axial locations, $x/L = 0.175$, 0.392, and 0.608, respectively, to measure the local total lifting pressure. Each load cell is rigidly attached with a sensing piston (diameter ~12.7 mm) which can freely move through the planing surface to make a direct contact with the porous media. Hence the total lifting force from both the air and the solid phase is measured. By dividing this force with the sensing piston area, the local total lifting pressure was obtained. Because the leading and trailing edges are exposed to the atmosphere, the pore pressure at these locations is equal to zero gauge pressure and the total lifting pressure are only from the solid phase. To measure the solid phase lifting force, one turns off the motor and slowly and incrementally lowers the planing surface with no angle of attack. Thus, no pore pressure is generated. The solid phase lifting force is then measured as a function of the compression, which is used to estimate the total lifting pressure at $x/L = 0$ and 1, respectively. Six pressure sensors, P_i ($i = 1, 2, 3, 4, 5, 6$) (Silicon Microstructures, Inc., SM5652-015-G-3-LR), are evenly mounted on the planing plate at $x/L = 0.033$ for P_1, 0.167 for P_2, 0.3 for P_3, 0.63 for P_4, 0.8 for P_5, and 0.967 for P_6. Because of the elimination of lateral pressure, these pressure sensors are mounted off the centerline to make room for the load cells.

Another load cell, L_4 (Futek, model LSB200), is mounted on the motor to capture any torque that is applied to it, as shown in Fig. 1(b). Without the load cell, the motor is mounted with no constraint in the rotation direction, meaning that any torque applied to the motor will be transferred to the load cell. The total torque, $T = Fd$ where F is the reading of L_4 and d is the horizontal distance between L_4 and the rotation center of the motor, includes the following: (1) the torque used to overcome the friction associated with turning the rollers when the motor is turned on, T_0; (2) the one due to the friction force, F_2, between supporting board and running belt, $T_2 = F_2 d_2$, where d_2 is the radius of the roller; and (3) the torque due to the friction, F_1, between the porous layer and the planing surface, $T_1 = F_1 d_1$, where $d_1 = d_2 + (h_2 - h_1)/2$. T_0 is obtained by running the motor with the planing surface removed from the porous layer. $F_2 = \eta_2 L_t$ where L_t is the total lifting force generated inside the porous layer that is obtained from the area integration of the total pressure

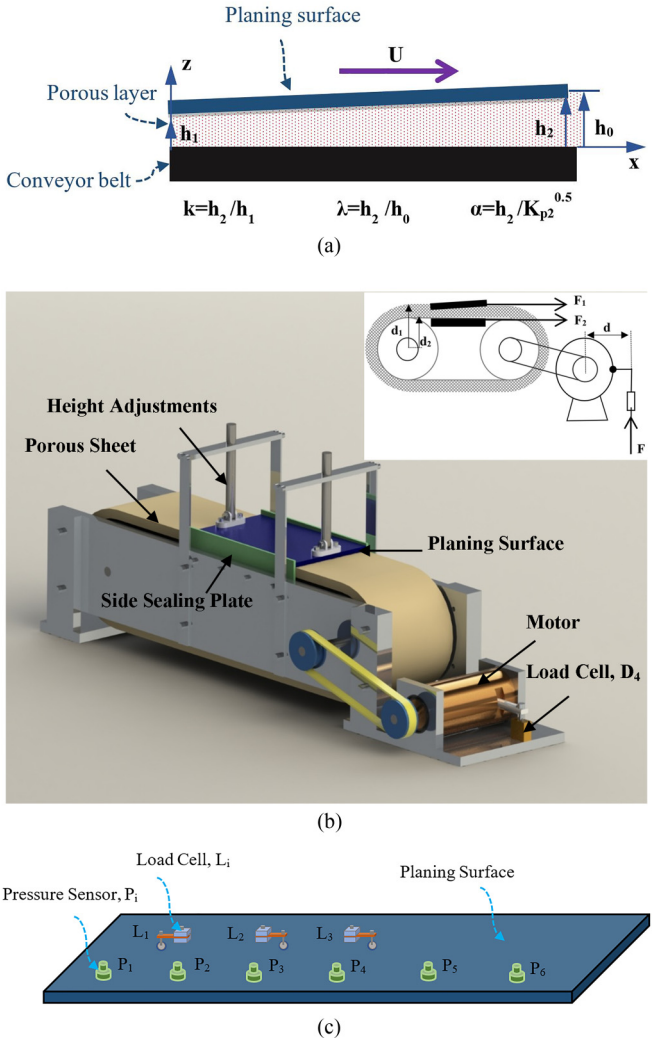

FIG. 1. Experimental setup for soft porous lubrication. (a) Problem schematic. A planing surface glides over a soft porous layer with a tilt angle at velocity U. The porous layer thicknesses under the trailing and leading edges are h_1 and h_2, respectively, and the undeformed porous layer thickness is h_0. For displaying purposes, this figure doesn't represent the accurate dimensional proportion in the experiments. (b) Experimental design. A fibrous porous layer is attached to a conveyor belt, and a planar board is held fixed above the porous layer serving as the planing surface. The conveyor belt is driven by two rollers connected to a DC electric motor. (c) The arrangement of the pressure sensors, P_i, and the load cells, L_i, on the planing surface.

distribution, and η_2 is the sliding friction coefficient between the running belt and the supporting board that is measured separately using a standard kinetic friction measurement setup. With T_0 and T_2 determined, one obtains the sliding friction coefficient between the porous layer and the planing surface, $\eta_1 = F_1/L_t = (Fd - T_0 - \eta_2 L_t d_2)/(d_1 L_t)$.

III. RESULTS

Figure 2(a) shows a representative result for the distributions of pore pressure and total lifting pressure along the axial direction of the planing surface, when $U = 4.5\,\mathrm{m/s}$, $L = 0.381\,\mathrm{m}$,

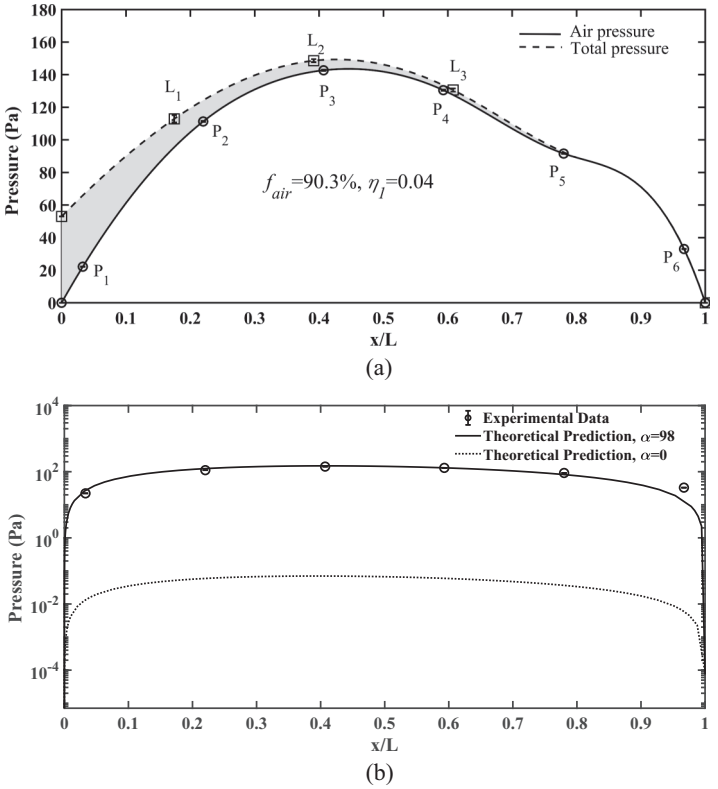

FIG. 2. (a) Representative time-averaged pore pressure distribution (measured by pressure sensors P_i) and total lifting pressure distribution (measured by load cells L_i) from trailing edge at $x/L = 0$ to leading edge at $x/L = 1$. (b) Comparison between experimental results and theoretical predictions in pore pressure generation. The belt with porous sheet attached on was running at a constant velocity $U = 4.5\,\mathrm{m/s}$. The length of the planing plate, $L = 0.381\,\mathrm{m}$. The porous layer thickness is $h_2 = h_0 = 19\,\mathrm{mm}$, $h_1 = 13\,\mathrm{mm}$. The Brinkman parameter at the leading edge, $\alpha = h_2/K_p^{0.5} = 98$. Under the running condition, the experiment was repeated three times. The error bars show that the variations in the measured pore pressure are below 5 Pa, which is close to the experimental error of the pressure sensors due to their calibrations.

$h_2 = h_0 = 1.9\,\mathrm{cm}$, $\lambda = h_2/h_0 = 1$, and $k = h_2/h_1 = 1.5$. There is no compression at $x/L = 1$, $K_{p2} = 3.70 \times 10^{-8}\ \mathrm{m}^2$, thus $\alpha = h_2/K_{p2}^{0.5} = 98$. It is noticed that this value of α is exactly in the same order as that observed in the EGL [6]. The distribution of the pore pressure was obtained by curve fitting through the readings of P_i and the zero gauge pressure at $x/L = 0$ and 1, respectively. The distribution of the total pressure was obtained by curve fitting through the readings L_i, along with the lifting pressure only from the solid phase at $x/L = 0$ and 1, respectively. It suggests in Fig. 1(a) that the pore pressure smoothly grows from $x/L = 1$, reaches its peak at $x/L = 0.45$, and then relaxes to the zero gauge pressure at $x/L = 0$. The compression of the porous layer due to the angle of the attack of the planing surface causes the porosity to continually decrease, from 0.994 at $x/L = 1$ to 0.991 at $x/L = 0$. Accordingly, the permeability dramatically decreases from $3.70 \times 10^{-8}\ \mathrm{m}^2$ to $1.86 \times 10^{-8}\ \mathrm{m}^2$ [29]. Lower permeability leads to higher flow resistance for the transiently trapped air to escape, and thus a higher pore pressure is generated. Because the trailing edge, $x/L = 0$, is exposed to the atmosphere, the peak pore pressure occurs at $x/L = 0.45$. Compared with the pore pressure, the total pressure shows a similar growth from the zero gauge pressure at $x/L = 1$ to the peak pressure at $x/L = 0.43$. Unlike the pore pressure, after the peak value, the total pressure decreases to a nonzero pressure at the $x/L = 0$, which is purely from the

solid phase lifting force. The area integration of the pore pressure and total pressure leads to the overall lifting force from the pore pressure, $L_p = WL\int_0^1 P(x/L)\,d(x/L)$, and that from the total pressure, $L_t = WL\int_0^1 P_t(x/L)\,d(x/L)$, respectively. Here W is the width of the planing surface; $P(x/L)$ and $P_t(x/L)$ are the distributions of the pore pressure and total pressure, respectively, shown in Fig. 2(a). Hence, the solid phase lifting force, $L_s = L_t - L_p$, is presented by the shaded area in Fig. 2(a). The overall contribution of the transiently trapped air to the total lift is given by $f_{\text{air}} = L_p/L_t$. Under the running condition in Fig. 2(a), $f_{\text{air}} = 90.3\%$, indicating that the planing surface is mainly supported by the air trapped inside the porous media. The sliding friction coefficient between the planing surface and the porous layer is measured, $\eta_1 = 0.04$. To achieve a smooth and low friction riding, one aims to increase the f_{air} and decrease the η_1.

The theoretical prediction from Ref. [6] for the pore pressure distribution under the planing surface, in the case of large α and without lateral pressure leakage, is reduced to

$$\frac{d}{dx'}\left[-\frac{h'}{\alpha(x')^2}\frac{dP'}{dx'}\right] = \frac{dh'}{dx'}, \tag{1}$$

where $x' = x/L$, $h' = h/h_2$, and $P' = Ph_2^2/(\mu UL)$. Here μ is the dynamic viscosity of the fluid; h is the thickness of the porous layer at different locations, x. The theoretical prediction under the representative running conditions ($\alpha = 98$) of Fig. 2(a) is presented in Fig. 2(b). Excellent agreement between the theoretical results with the experimental data is observed. Consistent results were obtained for other running conditions, conclusively demonstrating the validity of the theory. To demonstrate the significant role of the soft porous structure in the lift generation, we also plot in Fig. 2(b) the theoretical prediction of the fluid pressure distribution under the same running condition but without porous material, $\alpha = 0$. It is clearly shown in this figure that, when α changes from 0 to 98, the generated fluid pressure is increased by four orders of magnitude, revealing the key physics of soft porous lubrication.

A parametric study (U, k, λ, L, and material) was performed by varying one parameter while keeping all others constant.

Table I shows that a higher velocity, U, leads to a higher contribution of the pore pressure to the total lift, f_{air}, and a lower friction coefficient, η_1. It was shown in Refs. [6,13] that the pore pressure generation is proportional to the velocity, U. The faster the compression is, the more pore pressure is generated. On the other hand, the solid phase lifting force, L_s, is mainly dependent on the compression ratio k and precompression λ [28]. With k and λ fixed, L_s remains almost unchanged. Thus, when U is increased from 2.5 m/s to 5.0 m/s, f_{air} increased from 58% to 79.6%. Correspondingly, η_1 is decreased tremendously, from 0.44 to 0.06, an order of magnitude decreases.

Table I shows that a smaller compression ratio leads to a higher f_{air} and a lower η_1. When the angle of attack is decreased from 4 to 1.5, f_{air} is increased from 63.2% to 86.5%, and η_1 is decreased from 0.45 to 0.1. The higher value of k causes the decrease in the Darcy permeability [26,29], and hence the increase in the resistance that the fluid encounters as it escapes to the surroundings, higher pore pressure is generated as a result. The higher value of k also leads to the increase of the solid phase pressure, which exceeds the increase of pore pressure. Thus, f_{air} is decreased.

Table I shows that, when λ is increased from 0.8 to 1.0, less compression occurs at $x/L = 1$, and L_s decreases significantly. As a result, f_{air} increased from 49.9% to 67.8% and η_1 decreased by almost 50%, from 0.59 when $\lambda = 0.8$ to 0.29 when $\lambda = 1$.

A better lubrication effect is observed with a longer planing plate. Table I shows that, when L is increased from 0.381 m to 0.546 m, f_{air} increased from 67.8% to 80.5% and η_1 decreased from 0.29 to 0.10. The longer plate means a longer distance for the trapped air to escape. The characteristic time for the pore pressure to relax is proportional to the square of the characteristic length [11,12]. Thus, with larger L, more air is trapped inside the porous layer, and higher pore pressure is generated. On the other hand, L_s is not changed because the compression of the porous media remains unchanged. The overall result is a significantly increased f_{air} and thus reduced η_1.

TABLE I. The summarized experimental data for a parametric study of soft porous lubrication, showing the contribution of the pore pressure to the total lift, f_{air}, and the friction coefficient η_1 as a function of different running conditions (U, $\lambda = h_2/h_0$, $k = h_2/h_1$, L, and material). Under the same running condition, each experiment in the parametric study was repeated three times. The variations in f_{air} and η_1 are shown.

U (m/s)	λ	k	L (m)	Material	f_{air}	η_1
U dependence: Keeping k, λ, L, and material						
2.5	1.0	3	0.381	P	$58.0 \pm 0.4\%$	0.44 ± 0.02
3.3	1.0	3	0.381	P	$67.8 \pm 0.1\%$	0.29 ± 0.02
4.0	1.0	3	0.381	P	$72.7 \pm 0.3\%$	0.19 ± 0.02
4.5	1.0	3	0.381	P	$76.0 \pm 0.2\%$	0.14 ± 0.01
5.0	1.0	3	0.381	P	$79.6 \pm 0.2\%$	0.06 ± 0.02
k dependence: Keeping U, λ, L, and material						
3.30	1.0	4	0.381	P	$63.2 \pm 1.0\%$	0.45 ± 0.04
3.30	1.0	3	0.381	P	$67.8 \pm 0.1\%$	0.29 ± 0.02
3.30	1.0	2	0.381	P	$70.2 \pm 0.5\%$	0.13 ± 0.02
3.30	1.0	1.5	0.381	P	$86.5 \pm 1.4\%$	0.10 ± 0.02
λ dependence: Keeping U, k, L, and material						
3.30	1.0	3	0.381	P	$67.8 \pm 0.1\%$	0.29 ± 0.02
3.30	0.9	3	0.381	P	$57.6 \pm 0.3\%$	0.44 ± 0.02
3.30	0.8	3	0.381	P	$49.9 \pm 0.1\%$	0.59 ± 0.01
L dependence: Keeping U, k, λ, and material						
3.30	1.0	3	0.381	P	$67.8 \pm 0.1\%$	0.29 ± 0.02
3.30	1.0	3	0.451	P	$72.0 \pm 0.1\%$	0.15 ± 0.01
3.30	1.0	3	0.546	P	$80.5 \pm 0.8\%$	0.10 ± 0.02
Material dependence: Keeping U, k, λ, and L						
3.30	1.0	3	0.381	P	$67.8 \pm 0.1\%$	0.29 ± 0.02
3.30	1.0	3	0.381	F	$18.7 \pm 0.2\%$	0.54 ± 0.14
3.30	1.0	3	0.381	W	$29.0 \pm 0.2\%$	0.42 ± 0.01

To examine the effect of the material stiffness on the soft porous lubrication, we chose two other fibrous porous materials: "material F" (100% polyester fibers) and "material W" (100% wool). They shared the same fiber diameter ($\sim$30 μm), initial porosity ($\sim$0.994), and thus similar permeability behavior [29]. A static compression test was performed, showing that material W is much softer than material F (e.g., under the same static load, 1000 Pa, the strain of material W is 16% more than that of material F). Under the same running conditions ($k = 3$, $\lambda = 1$, $U = 3.3$ m/s, $h_2 = 19$ mm, and $L = 0.381$ m), the pore pressure distribution in these two materials is very close to each other due to their similar permeability values [6]. However, higher total pressure is generated in material F because it is stiffer, thus, f_{air} is lower (18.7%) and the corresponding η_1 is higher (0.54) for material F, as shown in Table I. This comparison clearly demonstrates that softer porous materials are favorable for improving the lubrication effect.

Figure 3 shows the dependence of η_1 as a function of f_{air} under different running conditions of material P. In general, η_1 decreases monotonically with the increase of f_{air}. This is because the frictional force is proportional to the lifting force from the solid phase only. With more of the load supported by the pore pressure, the solid phase lifting force decreases and so does the friction coefficient. Thus, the key for establishing a superlubrication condition with minimum frictional loss is via increasing the pore pressure's contribution to the total lift, f_{air}. The parametric study shown in Table I indicates that f_{air} is increased with higher running velocity, U, longer pressure relaxation distance, L, softer material, and smaller compression of the porous layer. In the current study, we were able to obtain a sliding friction coefficient as low as 0.04 when $U = 4.5$ m/s, $L = 0.381$ m,

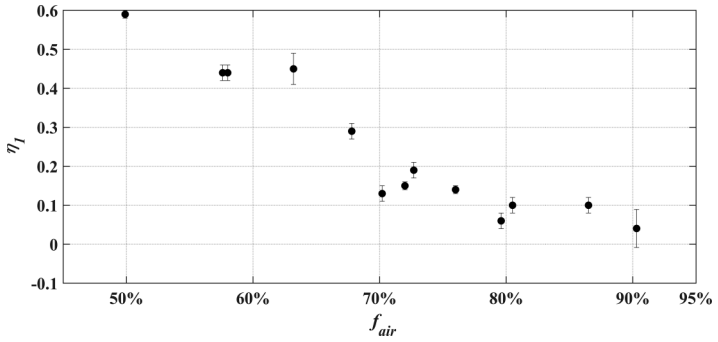

FIG. 3. f_{air} versus η_1 for "material P." f_{air} is the pore pressure's contribution to the total lift. η_1 is the friction coefficient between the planing surface and the porous sheet. Under the same running conditions, each experiment in the parametric study was repeated three times. The error bars are plotted for showing its repeatability.

$\lambda = 1$, and $k = 1.5$ for material P. In practical applications, η_1 can be lowered much further. In particular, synthetic fibrous materials were used herein, while, in practical applications, functionalized fibrous material such as a supramolecular porous layer (SML) can be used. The fiber diameter of the SML is at least one order of magnitude smaller than the synthetic fibers. Hence the material is much softer with much lower permeability [29], which allows larger value of f_{air} and smaller η_1. It is also noticed that the pore fluid in the current study is air, while in practical applications, highly viscous lubricant is used, which could significantly increase the pore fluid pressure.

Inspired by the exquisite design of the EGL and its critical role in establishing the superlubrication condition when a RBC glides over it, we report in this paper an experimental study about soft porous lubrication. The use of the soft fibrous porous media as a type of bearing not only improves the lubrication effect by transiently trapping more fluid inside, it also prevents direct contact between two moving objects and thus serves as a buffering layer. The study presented herein has the potential to substantially improve our understanding of the behavior of highly compressible porous media as a lubricating layer with vastly increased lift and reduced drag. It could dramatically change existing approaches to superlubricating films and result in substantial savings in energy consumption and thus reduction in greenhouse gas emissions. It also provides very critical insights in the biophysical study of the EGL, the articular cartilage, and other soft tissues in biological systems.

ACKNOWLEDGMENTS

The authors would like to acknowledge Dr. Rungun Nathan, Dr. Robert Crawford, Thomas Gacka, and Qiuyun Wang for their help during the experiments and Jennifer Muller for proofreading the manuscript. The technical support from Chris Townend and Zach Nowasad is greatly appreciated. This research was supported by the National Science Foundation under Award No. 1511096.

[1] K. Holmberg, P. Andersson, and A. Erdemir, Global energy consumption due to friction in passenger cars, Tribol. Int. **47**, 221 (2012).

[2] H. Vink and B. R. Duling, Identification of distinct luminal domains for macromolecules, erythrocytes, and leukocytes within mammalian capillaries, Circulation Res. **79**, 581 (1996).

[3] A. R. Pries, T. W. Secomb, and P. Gaehtgens, The endothelial surface layer, Pflügers Arch. - Eur. J. Physiol. **440**, 653 (2000).

[4] S. Weinbaum, J. M. Tarbell, and E. R. Damiano, The structure and function of the endothelial glycocalyx layer, Annu. Rev. Biomed. Eng. **9**, 121 (2007).
[5] T. W. Secomb, Blood flow in the microcirculation, Annu. Rev. Fluid Mech. **49**, 443 (2017).
[6] J. Feng and S. Weinbaum, Lubrication theory in highly compressible porous media: The mechanics of skiing, from red cells to humans, J. Fluid Mech. **422**, 282 (2000).
[7] T. W. Secomb, R. Hsu, and A. R. Pries, Motion of red blood cells in a capillary with an endothelial surface layer: Effect of flow velocity, Am. J. Physiol. Heart Circ. Physiol. **281**, H629 (2001).
[8] T. W. Secomb, R. Hsu, and A. R. Pries, Effect of the endothelial surface layer on transmission of fluid shear stress to endothelial cells, Biorheology **38**, 143 (2001).
[9] S. Weinbaum, X. Zhang, Y. Han, H. Vink, and S. C. Cowin, Mechanotransduction and flow across the endothelial glycocalyx, Proc. Natl. Acad. Sci. USA **100**, 7988 (2003).
[10] J. M. Squire, M. Chew, G. Nneji, C. Neal, J. Barry, and C. Michel, Quasi-periodic substructure in the microvessel endothelial glycocalyx: A possible explanation for molecular filtering? J. Struct. Biol. **136**, 239 (2001).
[11] Q. Wu, Y. Andreopoulos, and S. Weinbaum, From Red Cells to Snowboarding: A New Concept for a Train Track, Phys. Rev. Lett. **93**, 194501 (2004).
[12] Q. Wu, Y. Andreopoulos, S. Xanthos, and S. Weinbaum, Dynamic compression of highly compressible porous media with application to snow compaction, J. Fluid Mech. **542**, 281 (2005).
[13] Q. Wu, Y. Igci, Y. Andreopoulos, and S. Weinbaum, Lift mechanics of downhill skiing and snowboarding, Med. Sci. Sports Exer. **38**, 1132 (2006).
[14] Q. Wu and Q. Sun, A comprehensive skiing mechanics theory with implications to snowboard optimization, Med. Sci. Sports Exer. **43**, 1955 (2011).
[15] J. M. Skotheim and L. Mahadevan, Soft Lubrication, Phys. Rev. Lett. **92**, 245509-1 (2004).
[16] J. M. Skotheim and L. Mahadevan, Soft lubrication: The elastohydrodynamics of nonconfirming and conforming contacts, Phys. Fluids **17**, 092101 (2005).
[17] P. Mirbod, Y. Andreopoulos, and S. Weinbaum, On the generation of lift forces in random soft porous media, J. Fluid Mech. **619**, 147 (2009).
[18] Q. Wu, Y. Andreopoulos, and S. Weinbaum, in *The Engineering of Sport 6*, edited by E. F. Moritz and S. Haake (Springer, New York, 2006), pp. 281–286.
[19] Q. Wu and S. Ganguly, in *The Impact of Technology on Sport II*, edited by F. K. Fuss, A. Subic, and S. Ujihashi (Taylor and Francis, New York, 2007), pp. 833–838.
[20] Q. Wu and Q. Sun, in *The Engineering of Sport 7*, edited by M. Estivalet and P. Brisson (Springer, Paris, 2008), pp. 457–465.
[21] Q. Wu and Q. Sun, in *Science and Skiing IV*, edited by E. Müller, S. Lindinger, and T. Stöggl (Meyer & Meyer Sport (UK), New York, 2009), pp. 708–717.
[22] M. Al-Chidiac, P. Mirbod, Y. Andreopoulos, and S. Weinbaum, Dynamic compaction of soft compressible porous materials: Experiments and air-solid phase interaction, J. Porous Media **12**, 1019 (2009).
[23] B. Barabadi, R. Nathan, K. Jen, and Q. Wu, On the characterization of lifting forces during the rapid compaction of deformable porous media, J. Heat Transfer **131**, 101006 (2009).
[24] R. Crawford, R. Nathan, K. P. Jen, and Q. Wu, Dynamic compression of soft porous media: From finite to infinite domain, J. Porous Media **14**, 51 (2011).
[25] R. Crawford, G. F. Jones, L. You, and Q. Wu, Compression-dependent permeability measurements for random soft medium and its implications to lift generation, Chem. Eng. Sci. **66**, 294 (2011).
[26] R. Crawford, R. Nathan, L. Wang, and Q. Wu, Experimental study on the lift generation inside a random synthetic porous layer under rapid compaction, Exp. Therm. Fluid Sci. **36**, 205 (2012).
[27] Q. Wu, S. Santhanam, R. Nathan, and Q. Wang, A biphasic approach for the study of lift generation in soft porous media, Phys. Fluids **29**, 043602 (2017).
[28] T. Gacka, Z. Zhu, R. Crawford, R. Nathan, and Q. Wu, From red cells to soft lubrication, an experimental study of lift generation inside a compressible porous layer, J. Fluid Mech. **818**, 5 (2017).
[29] Z. Zhu, Q. Wang, and Q. Wu, On the examination of the Darcy permeability of soft fibrous porous media: New correlations, Chem. Eng. Sci. **173**, 525 (2017).